Image denoising based on gaussian/bilateral filter and its method noise thresholding

B. K. Shreyamsha Kumar

Abstract The Gaussian filter is a local and linear filter that smoothes the whole image irrespective of its edges or details, whereas the bilateral filter is also a local but non-linear, considers both gray level similarities and geometric closeness of the neighboring pixels without smoothing edges. The extension of bilateral filter: multi-resolution bilateral filter, where bilateral filter is applied to approximation subbands of an image decomposed and after each level of wavelet reconstruction. The application of bilateral filter on the approximation subband results in loss of some image details, whereas that after each level of wavelet reconstruction flattens the gray levels thereby resulting in a cartoon-like appearance. To tackle these issues, it is proposed to use the blend of Gaussian/bilateral filter and its method noise thresholding using wavelets. In Gaussian noise scenarios, the performance of proposed methods is compared with existing denoising methods and found that, it has inferior performance compared to Bayesian least squares estimate using Gaussian Scale mixture and superior/comparable performance to that of wavelet thresholding, bilateral filter, multi-resolution bilateral filter, NL-means and Kernel based methods. Further, proposed methods have the advantage of less computational time compared to other methods except wavelet thresholding, bilateral filter.

Keywords Gaussian filter · Bilateral filter · Method noise · Wavelet thresholding · Bayes shrink · Multi-resolution bilateral filter

B. K. Shreyamsha Kumar (✉)
Central Research Laboratory, Bharat Electronics,
Bangalore 560013, India
e-mail: shreyamsha@yahoo.com

Abbreviations

BF	Bilateral filter
GFMT	Gaussian filter and its Method noise thresholding
BFMT	Bilateral filter and its Method noise thresholding
MRBF	Multi-resolution bilateral filter
NL-means	Non local-means
WT	Wavelet transform
MSE	Mean-squared error
SURE	Stein unbiased risk estimator
BLS-GSM	Bayesian least squares estimate using Gaussian Scale mixture

1 Introduction

Scientific data sets collected by sensors always suffer from perturbations in the sense that there is a superposition of noise and the signal in question. This is because of data acquisition and/or transmission system, which can degrade the signal of interest. A first preprocessing step in analyzing such data sets is denoising, that is, estimating the signal of interest from the available noisy data [1].

Denoising has long been a focus of research and yet there always remains room for improvement, especially in image denoising. The simple spatial filtering of a corrupted image can be successful when high frequency noise is to be removed from the corrupted image. The main difficulty associated with this is, the computational complexity involved in performing the convolution. Frequency-domain methods overcome these problems due to the Fourier convolution property where convolution is transformed into multiplication of the spectra. As the noise is spread across all frequencies, the frequency-based denoising methods adopt low-pass filtering to

suppress most of high-frequency components in order to denoise the image. However, this is generally not effective as it suppresses both noise as well as other high-frequency features of the image, resulting in an overly smoothed denoised image.

Many of the denoising methodologies and strategies [2–13] devise a model for the noise and/or for the original signal in a suitable subspace where the differences between them are accentuated based on the following observations: (1) the noise and clean signal show different behaviors in multiresolution representation, (2) significant geometrical components of an image (edges) or time structures of a signal (sharp transitions) over-exceed noise information, especially at low resolutions [14]. Hence, in last two decades, a flurry of research has involved the use of the wavelet transform for denoising because of its energy compaction and multiresolution properties [15,16]. The influential works on signal denoising via wavelet thresholding or shrinkage of Donoho and Johnstone [10,11] in the additive white Gaussian noise setting have shown that various thresholding schemes for denoising have near-optimal properties in the minimax sense. The idea of wavelet thresholding is in the assumption that the signal magnitudes increasingly dominate the magnitudes of the noise in a wavelet representation with increasing level, so that wavelet coefficients can be set to zero if their magnitudes are less than a predetermined threshold. The most popular thresholding schemes for denoising are hard-thresholding and soft-thresholding methods, where the former leaves the magnitudes of coefficients unchanged if they are larger than a given threshold, while the latter just shrinks them to zero by the threshold value otherwise it is set to zero in both cases. Even though soft-thresholding introduces more error or bias than hard-thresholding, it is more efficient in denoising. But for some classes of images hard-thresholding performs better [3].

However, the major problem with both methods and most of their variants is the choice of a suitable threshold value. Initially, Donoho and Johnstone have given a mechanism for finding a universal threshold value known as VisuShrink, which depends on the noise power and the signal size (number of samples in the image). It follows the global thresholding scheme where there is a single value of threshold applied globally to all the wavelet coefficients. As the given noisy signal may consist of some parts where the magnitudes of the signal are below the threshold and other parts where the noise magnitudes are above the given threshold, thresholding by VisuShrink will cut off parts of the signal on one hand and leave some noise untouched on the other hand. This observation has led to the idea of a non-uniform or adaptive threshold depending on the relationship between the energy distribution of the observed signal and that of the noise. The use of different thresholds for different decomposition levels and subbands seems more reasonable as the adaptive threshold

accounts for variation of the local statistics of the wavelet coefficients.

Donoho and Johnstone developed an adaptive method of selecting a threshold that adapts to the data as well as minimizing the Stein unbiased risk estimator (SURE), which is known as the SureShrink wavelet thresholding technique [10,17]. This is achieved by choosing distinct thresholds for each subband of each decomposition level of the wavelet tree using an efficient recursive process [2]. This thresholding scheme attempts to select thresholds that adapt to the data as well as minimize an estimation of the MSE or risk. Further, it uses a hybrid approach while selecting the SURE threshold or local universal threshold depending on the energy of the particular subband. That is, it uses SURE threshold in high activity subbands and localized universal threshold in sparse subbands. Although the SureShrink thresholding method clearly provides an adaptive thresholding strategy, its performance is dependent on estimating the statistics of the wavelet coefficients of the original image from that of the noisy image. Further, Chang et al. has derived a threshold in a Bayesian framework assuming a generalized Gaussian distribution for the wavelet coefficients and called it BayesShrink [3]. This method has a better mean squared error (MSE) performance than SureShrink. These shrinkage methods have later been improved by considering inter-scale and intra-scale correlations of the wavelet coefficients [5,13,18]. The denoising method proposed in [18], known as BLS-GSM, models the neighborhoods of coefficients at adjacent positions and scales as Gaussian Scale Mixture (GSM), and applies the Bayesian Least Squares (BLS) estimation technique to update the wavelet coefficients. Further, kernel based image denoising proposed in [19] uses support vector regression to enforce the relations among natural image wavelet coefficients in the estimated signal.

Bilateral Filter proposed in [20] considers both spatial and intensity information between a point and its neighboring points, unlike the conventional linear filtering where only spatial information is considered. This preserves the edges/sharp boundaries very well while noise is averaged out as it average pixels belonging to the same region as the reference pixel. But it fails when the standard deviation of the noise exceeds the edge contrast. The concept of the Bilateral Filter was earlier presented in [21] as the SUSAN filter and in [22] as the neighborhood filter. Recently, many researchers have devoted to the modification and improvement of the classical Bilateral Filtering algorithm [23–27]. Further, the connection between Bilateral Filter and anisotropic diffusion has been established in [28]. Elad [29] proved that the Bilateral Filter is identical to a single Jacobi iteration of a weighted least squares minimization. In [30], Buades et al. proposes a nonlocal means (NL-means) filter, where pixel weights are determined using similarity of local patches. When the patch size is reduced to one pixel, the NL-means filter becomes

equivalent to the Bilateral Filter. Further, Kervrann et al. [31] extended the work of Buades et al. [30] by controlling the neighborhood of each pixel adaptively. In [32,33], the authors give an empirical study of the optimal Bilateral Filter parameter selection in image denoising applications and proposed the multi-resolution Bilateral Filter (MRBF). The application of bilateral filter on the approximation subband results in loss of some image details, whereas that after each level of wavelet reconstruction flattens the gray levels thereby resulting in a cartoon-like appearance. Further, the variants of MRBF proposed in [34] for denoising of magnetic resonance images, and in [35] for astronomical, ultrasound and X-ray images also suffers from loss of some image details and flattening of gray levels due to bilateral filter. This is because, the application of bilateral filter removes noise as well as some image details by spatial filtering without loss of edge information (range filtering). As an attempt to solve these issues, an amalgamation of Gaussian/Bilateral Filtering and its method noise thresholding using wavelets has been proposed for image denoising.

The paper is organized as follows: Sect. 2 discusses the Gaussian and Bilateral Filter, Sect. 3 proposes the Gaussian/Bilateral Filter and its method noise thresholding using wavelets for image denoising, Sect. 4 discusses experimental results, and conclusions follow in Sect. 5.

2 Gaussian and bilateral filter

The goal of image denoising is to remove the noise while retaining the important image features like edges, details as much as possible. Linear filters, which consist of convolving the image with a constant matrix to obtain a linear combination of neighborhood values, have been widely used for noise elimination in the presence of additive noise. However they can produce a blurred and smoothed image with poor feature localization and incomplete noise suppression.

Filters based on Gaussian functions are of particular importance because their shapes are easily specified and both the forward and inverse Fourier transforms of a Gaussian function are real Gaussian functions. Further if the frequency domain filter is narrower, the spatial domain filter will be wider which attenuates the low frequencies resulting in increased smoothing/blurring. These Gaussian filters are typical linear filters that have been widely used for image denoising. In Gaussian filters, weight of the pixels decays by distance from the center of the filter as given by

$$G_\sigma(x, y) = \frac{1}{2\pi\sigma^2} e^{-\frac{(x^2+y^2)}{2\sigma^2}} \qquad (1)$$

Gaussian filters assume that images have smooth spatial variations and pixels in a neighborhood have close values, by averaging the pixel values over a local neighborhood sup-

presses noise while preserving image features. However, this assumption fails at edges where the spatial variations are not smooth and the application of Gaussian filter blurs the edges. Bilateral filter overcomes this by filtering the image in both range and domain (space). Bilateral filtering is a local, nonlinear and non-iterative technique which considers both gray level (color) similarities and geometric closeness of the neighboring pixels. Mathematically, the bilateral filter output at a pixel location p is calculated as follows:

$$I_F(p) = \frac{1}{W} \sum_{q \in S} G_{\sigma_s}(\|p - q\|) G_{\sigma_r}(|I(p) - I(q)|) I(q)$$

$$(2)$$

where, $G_{\sigma_s}(\|p - q\|) = e^{-\frac{p-q^2}{2\sigma_s^2}}$ is a geometric closeness function,

$$G_{\sigma_r}(|I(p) - I(q)|) = e^{-\frac{|I(p)-I(q)|^2}{2\sigma_r^2}}$$

is a gray level similarity function,

$$W = \sum_{q \in S} G_{\sigma_s}(\|p - q\|) G_{\sigma_r}(|I(p) - I(q)|)$$

is a normalization constant,

$\|p - q\|$ is the Euclidean distance between p and q,

and S is a spatial neighborhood of p.

The two parameters σ_s and σ_r control the behavior of the bilateral filter. In [30], the dependency of σ_r/σ_s values and derivative of the input signal on the behaviors of the bilateral filter are analyzed. Also it is shown in [32] that, the optimal σ_s value is relatively insensitive to noise variance compared to the optimal σ_r value and is chosen based on the desired amount of low-pass filtering. A large σ_s blurs more, i.e., it combines values from more distant image locations. Also, if an image is scaled up or down, σ_s must be adjusted accordingly in order to obtain equivalent results. It appears that a good range for the σ_s value is roughly [1.5–2.1]; on the other hand, the optimal σ_r value changes significantly as the noise standard deviation σ_n changes. This is expected because if σ_r is smaller than σ_n, noisy data could remain isolated and untouched on the other hand if it is sufficiently large, σ_s becomes important; apparently increasing the value of σ_s results in over-smoothing. If the image is amplified or attenuated, σ_r must be adjusted accordingly in order to retain the same result.

3 Gaussian/bilateral filter and its method noise thresholding

The proposed scheme of image denoising uses the combination of Gaussian/Bilateral Filter and its Method noise Thresholding using wavelets (G/BFMT), and is shown in Fig. 1.

Fig. 1 Proposed image denoising framework
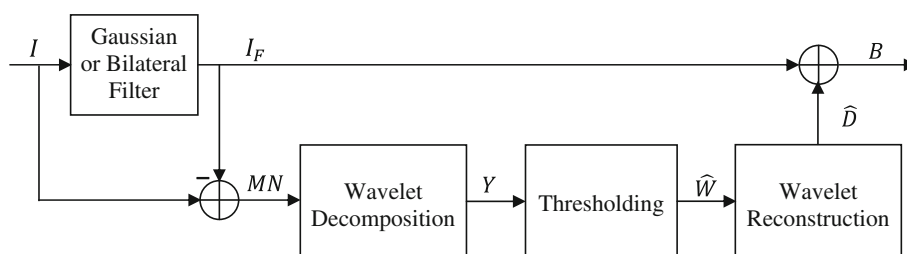
A difference between the original image and its denoised image shows the noise removed by the algorithm, which is called as method noise. In principle, the method noise should look like a noise. Since even good quality images have some noise, it makes sense to evaluate any denoising method in that way, without the traditional "add noise and then remove it" trick. Mathematically, it is given by

$$MN = A - I_F \tag{3}$$

where, A is the original image (not necessarily noisy) and I_F is the output of denoising operator for a input image A.

The application of bilateral filter on the noisy image averages the noise along with the image details while preserving edges/sharp boundaries very well provided the standard deviation of the noise is less than the edge contrast. In case of Gaussian filter, its method noise is zero in harmonic parts of the image and very large near edges or texture, where the Laplacian cannot be small. As a consequence, the Gaussian convolution is optimal in flat parts of the image but edges and texture are blurred. To capture what is removed from the noisy image by the Gaussian/Bilateral filter, the definition of the method noise is redefined as the difference between the noisy image and its denoised image. Hence, Eq. (3) is rewritten as

$$MN = I - I_F \tag{4}$$

where, $I = A + Z$ is a noisy image obtained by corrupting the original image A by a white Gaussian noise Z and I_F is the output of Gaussian/Bilateral filter for a input image I.

Since the Gaussian/Bilateral filter has removed the noise as well as image details by averaging the pixels, the method noise will consists of noise as well as image details along with some edges. The method noise due to Gaussian filtering will have more strong edges as compared to that of bilateral filtering as the edges are preserved by range filtering (σ_r). So, the method noise MN is a combination of image details D and a white Gaussian noise N and is written as

$$MN = D + N \tag{5}$$

Now the problem is to estimate the detail image D, which has only the original image features and edges/sharp boundaries that are removed by Gaussian/Bilateral filter, as accurately

as possible according to some criteria and is added with the Gaussian/Bilateral filtered image I_F to get better denoised image with details. In wavelet domain, Eq. (5) can be represented as

$$Y = W + N_w \tag{6}$$

where Y is the noisy wavelet coefficient (method noise), W is the true wavelet coefficient (detail image) and N_w is independent Gaussian noise.

In wavelet domain, the goal is to estimate the true wavelet coefficient W from Y by thresholding Y with a proper value of threshold which minimizes MSE so that it can retain the original image features and edges/sharp boundaries very well in the final denoised image. The estimate of the true wavelet coefficient is represented as $\widehat{W}$ and its wavelet reconstruction gives an estimate of detail image $\widehat{D}$. The summation of this detail image $\widehat{D}$ with the Gaussian/Bilateral filtered image I_F will give the denoised image B, certainly have more image details and edges as compared with Gaussian/Bilateral filtered image I_F.

Wavelet thresholding adds power to the proposed method as noise components can be eliminated better in detail subbands of method noise. As BayesShrink provides a better MSE performance than SureShrink, it is used in the proposed method to threshold the method noise wavelet coefficients. BayesShrink is also an adaptive, data-driven thresholding strategy via soft-thresholding which derives the threshold in a Bayesian framework assuming a generalized Gaussian distribution. This method is adaptive to each sub-band because it depends on data-driven estimates of the parameters. The threshold for a given subband derived by minimizing Bayesian risk and is given by

$$T = \frac{\sigma^2}{\sigma_w} \tag{7}$$

where σ^2 is the noise variance estimated from subband HH$_1$ by a robust median estimator [3] given by

$$\widehat{\sigma} = \frac{\text{Median}(|Y_{i,j}|)}{0.6745}, \quad Y_{i,j} \in \{\text{HH}_1\} \tag{8}$$

and σ_w^2 is the variance of wavelet coefficients in that subband, whose estimate is computed using

$$\widehat{\sigma}_w^2 = \max(\widehat{\sigma}_y^2 - \widehat{\sigma}^2, 0) \tag{9}$$

where $\widehat{\sigma}_y^2 = \frac{1}{MN} \sum_{i,j=1}^{M,N} Y_{i,j}^2$.

4 Results and discussion

Experiments were carried out on various standard grayscale images of size 256×256 which are shown in Fig. 2. The input images are corrupted by a simulated Gaussian white noise with zero mean and five different standard deviations $\sigma \in [10, 20, 30, 40, 50]$. The denoising process has been performed on these five noisy realizations. To validate the proposed methods (GFMT and BFMT), their performance are compared in terms of method noise, visual quality, PSNR, Image Quality Index (IQI) [35] and Visual Fidelity Index (VIF) [36] of the denoised images using the various methods available in literature such as Wavelet based Thresholding (WT), Bilateral Filtering (BF), MRBF [32], NL-means filtering [30], BLS-GSM [18] and Kernel based image denoising using support vector regression [19]. For NL-means filtering, BLS-GSM and Kernel based methods; the

parameter values suggested by the authors are used. In all the other cases, db8 is used for wavelet decomposition and BayesShrink soft thresholding is used to threshold these wavelet coefficients with exception of BF. In WT based thresholding, GFMT and BFMT three decomposition levels were used whereas in MRBF only one decomposition level is used. The remaining parameters used are given against the methods considered.

$\text{MRBF} : \sigma_s = 1.8, \sigma_r = \sigma_n, \text{neighborhoodwindow} = 11 \times 11$
$\text{BF} : \sigma_s = 1.8, \sigma_r = 5\sigma_n, \text{neighborhoodwindow} = 11 \times 11$
$\text{GFMT} : \sigma_s = 1.8, \text{neighborhoodwindow} = 11 \times 11$
$\text{BFMT} : \sigma_s = 1.8, \sigma_r = 5\sigma_n, \text{neighborhoodwindow} = 11 \times 11$

Any denoising algorithm should not alter the noise free images, so that the method noise should be very small when some kind of regularity for the image is assumed. The method noise of a very good image denoising method should look like a noise even for a noise free image. The method noise helps us to understand the performance and limitations of the denoising algorithms, since removed details or texture, edges have a large method noise. Figure 3 shows the performance of

Fig. 2 Original images used for experiments. **a** Lena, **b** Barbara, **c** Boat, **d** Baboon
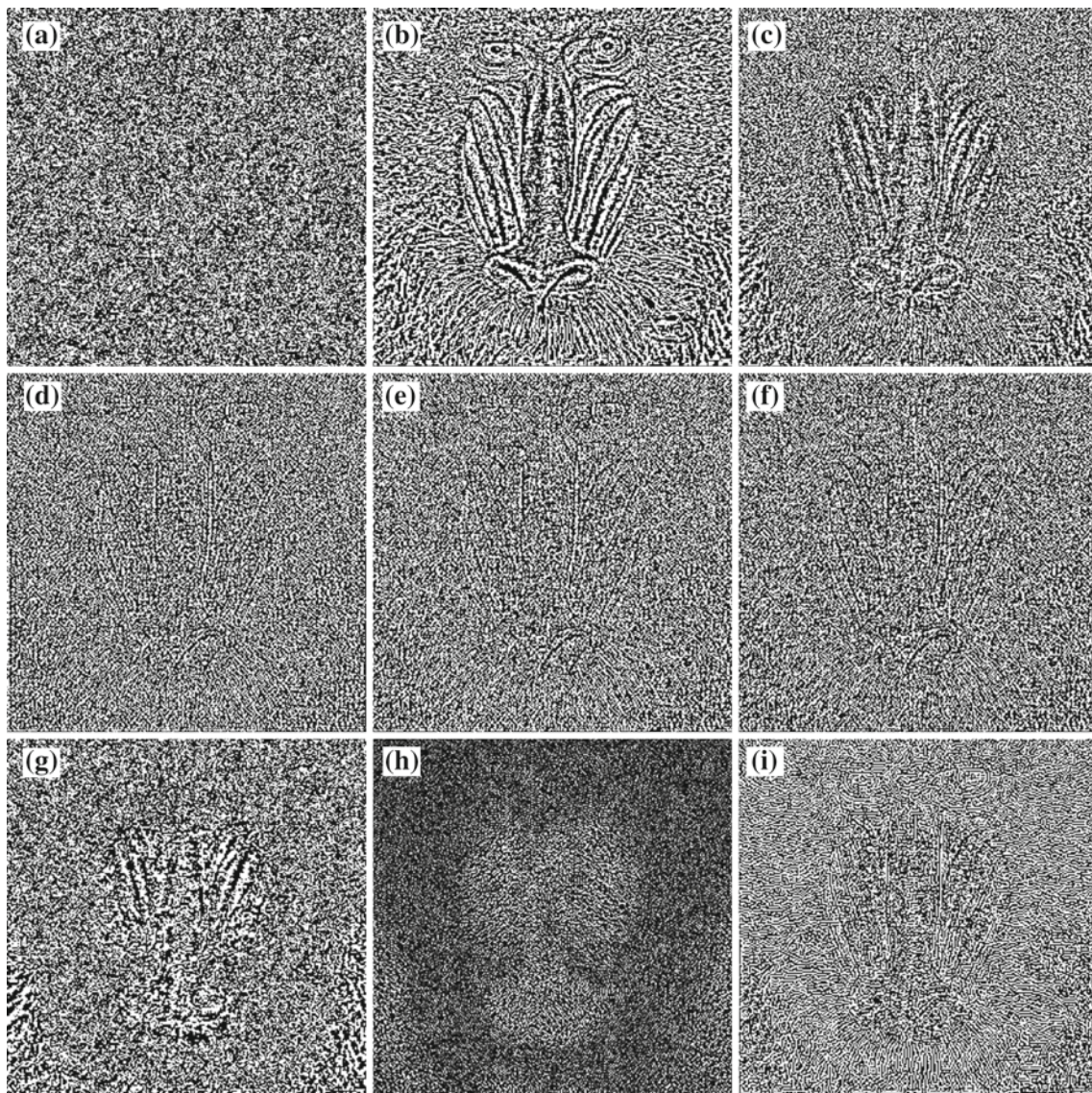
Fig. 3 Method noise of different denoising methods for an input noisy image of baboon with $\sigma = 2.5$. **a** Gaussian white noise of $\sigma = 2.5$, method noise of **b** BF, **c** MRBF, **d** WT, **e** GFMT, **f** BFMT, **g** NL-means, **h** BLSGSM, **i** Kernel based

the WT, BF, MRBF, the proposed methods (GFMT, BFMT), NL-means, BLS-GSM and Kernel based method in terms of method noise for an input image of baboon with $\sigma = 2.5$. It is observed from Fig. 3d–f that, the method noise of the WT and the proposed methods looks like a noise with very minimal image details, whereas that of MRBF has more details near the eyes and nose portions of baboon image (Fig. 3c). Fig. 3b shows the increased details throughout the method noise image which is due to BF. The wavelet thresholding of GF/BF's method noise (Fig. 3b) and its addition with GF/BF output improve the method noise of GFMT/BFMT respectively (Fig. 3e, f). That is, the image details present in the method noise of GF/BF (Fig. 3b) has been transferred to the denoised image of GFMT/BFMT and hence those details are not visible in the method noise of GFMT/BFMT (Fig. 3e, f).

Further it is observed that, NL-means (Fig. 3g) and Kernel based methods (Fig. 3i) also have the image details near nose portion of the image. The method noise of BLS-GSM (Fig. 3h) looks like noise only in some portions of the image (near nose and beard) and has some image details in other regions.

The minimum and maximum amplitude levels of the method noise are tabulated in Table 1 to compare the performance of the considered methods quantitatively. From Table 1 it is observed that, the minimum and maximum amplitudes of the method noise by BLS-GSM stand first in the list as they have lowest value (in absolute sense) compared to other methods. This is expected because of its outstanding denoising performance. If BLS-GSM is excluded from the comparison, then the proposed method, BFMT, has the lesser

**Table 1** Minimum and maximum amplitude levels of the method noise

Denoising methods	Minimum	Maximum
WT	**−11.4643**	12.7238
MRBF	−15.4956	17.3672
BF	−38.3523	39.4771
GFMT	**−11.4643**	13.7238
BFMT	**−11.4643**	**11.7238**
NL-means	−29.7921	28.3534
BLS-GSM	−6.3619	5.3672
Kernel based	−60.7738	58.2373

values thereby standing second in the list (bolded in Table 1). Also, both WT and GFMT have same minimum amplitude and is equivalent to that of BFMT. In terms of maximum amplitude, BFMT is followed by WT and then GFMT. It is noticed that, all the other methods have higher values with the last position shared by Kernel based method. From these observations it is found that, eventhough the performance of proposed methods is inferior to BLS-GSM, they have shown better performance compared to other methods in terms of method noise.

The image quality is measured by visual inspection as there is no generally accepted objective way to judge the image quality of a denoised image. There are two criteria that are used widely in the literature: (1) visibility of the artifacts, and (2) preservation of edge details. For image-quality comparison the baboon image is considered with different σ.

In all the Figs. 4, 5, 6, (a) shows noisy baboon image, the denoised images by BF, MRBF, WT, GFMT, BFMT, NL-
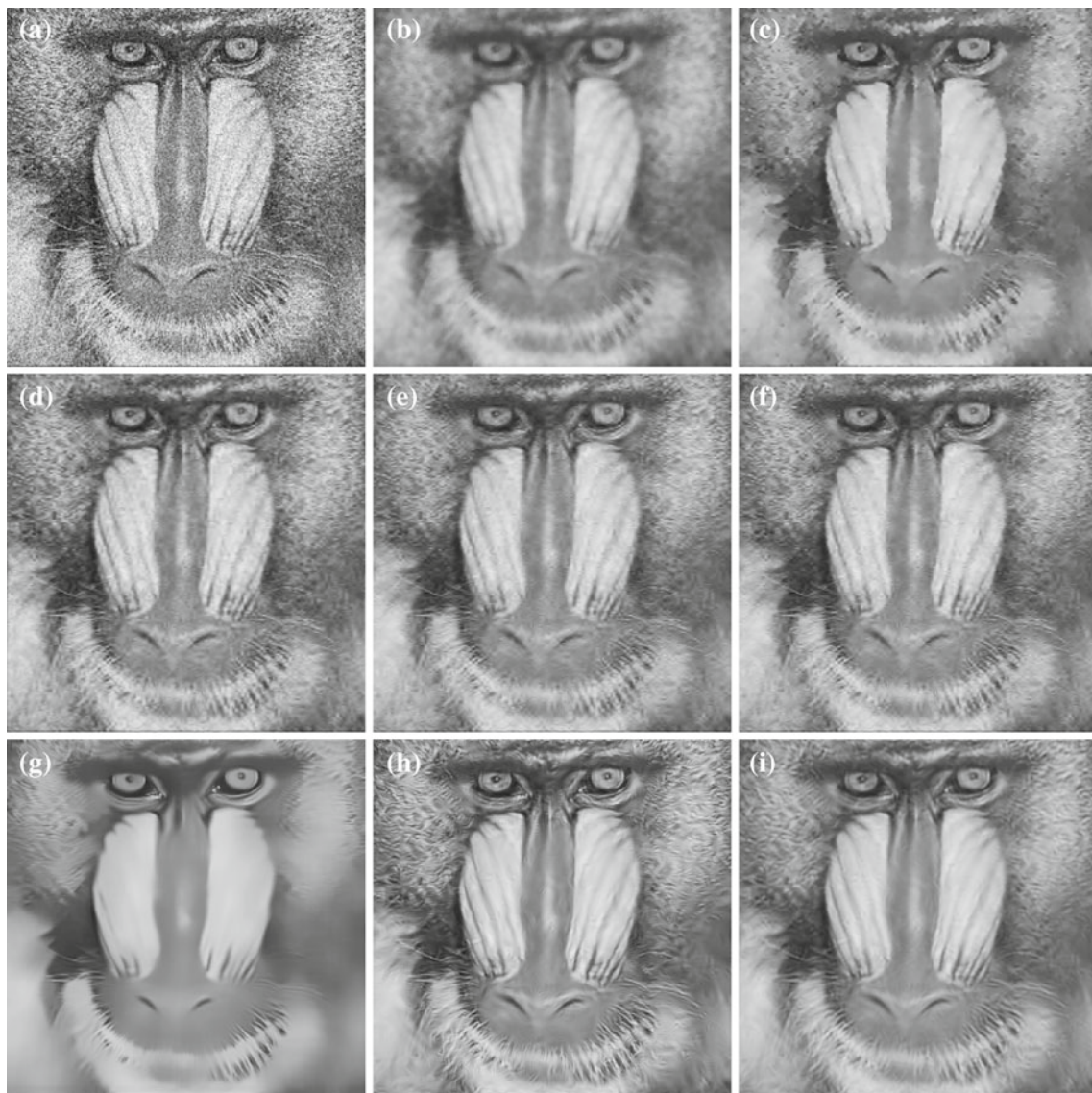
Fig. 4 Noisy baboon image with $\sigma = 20$ and its denoised images by different methods. **a** Noisy image with $\sigma = 20$, denoised images using **b** BF, **c** MRBF, **d** WT, **e** GFMT, **f** BFMT, **g** NL-means, **h** BLSGSM, **i** Kernel based
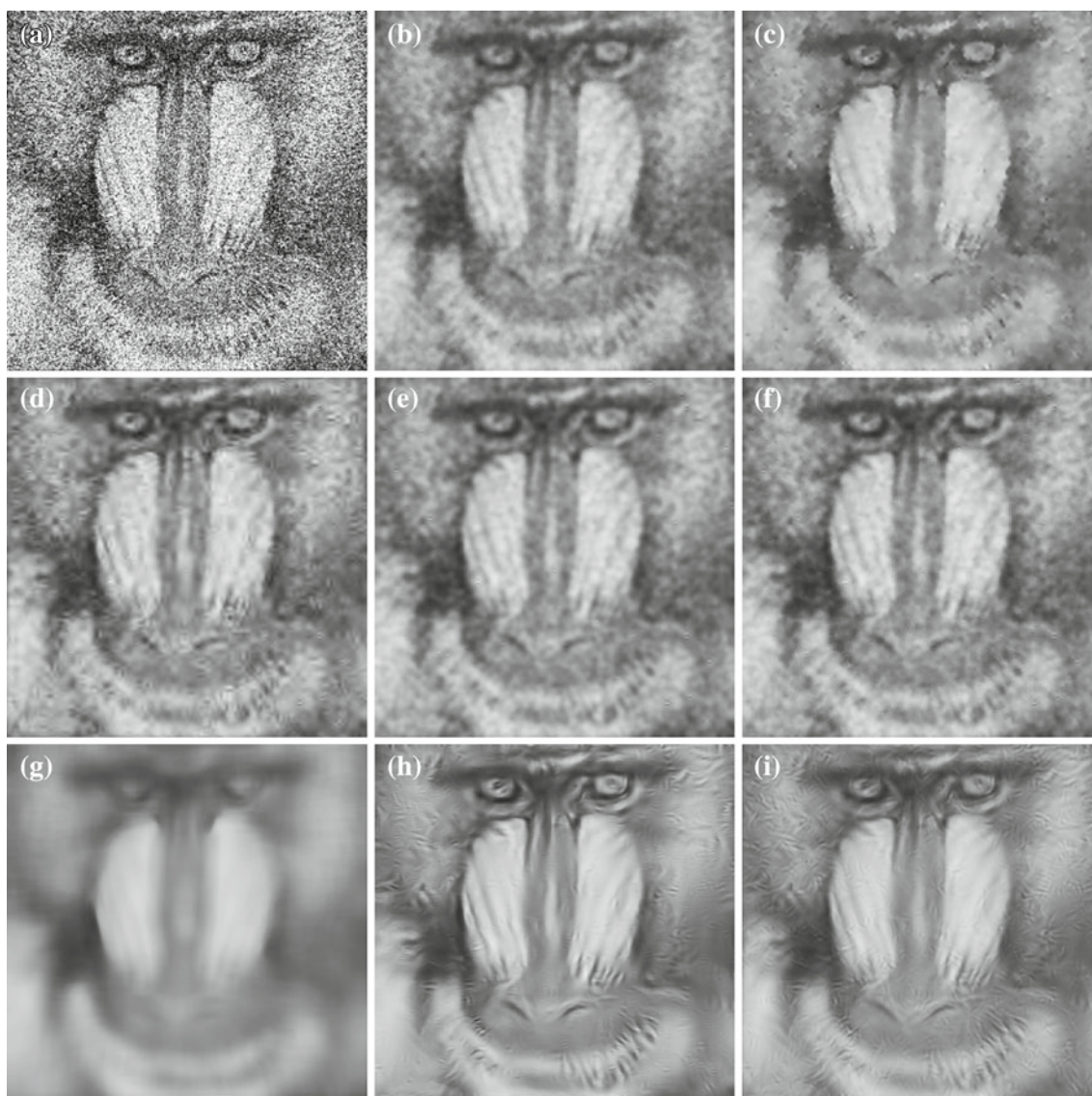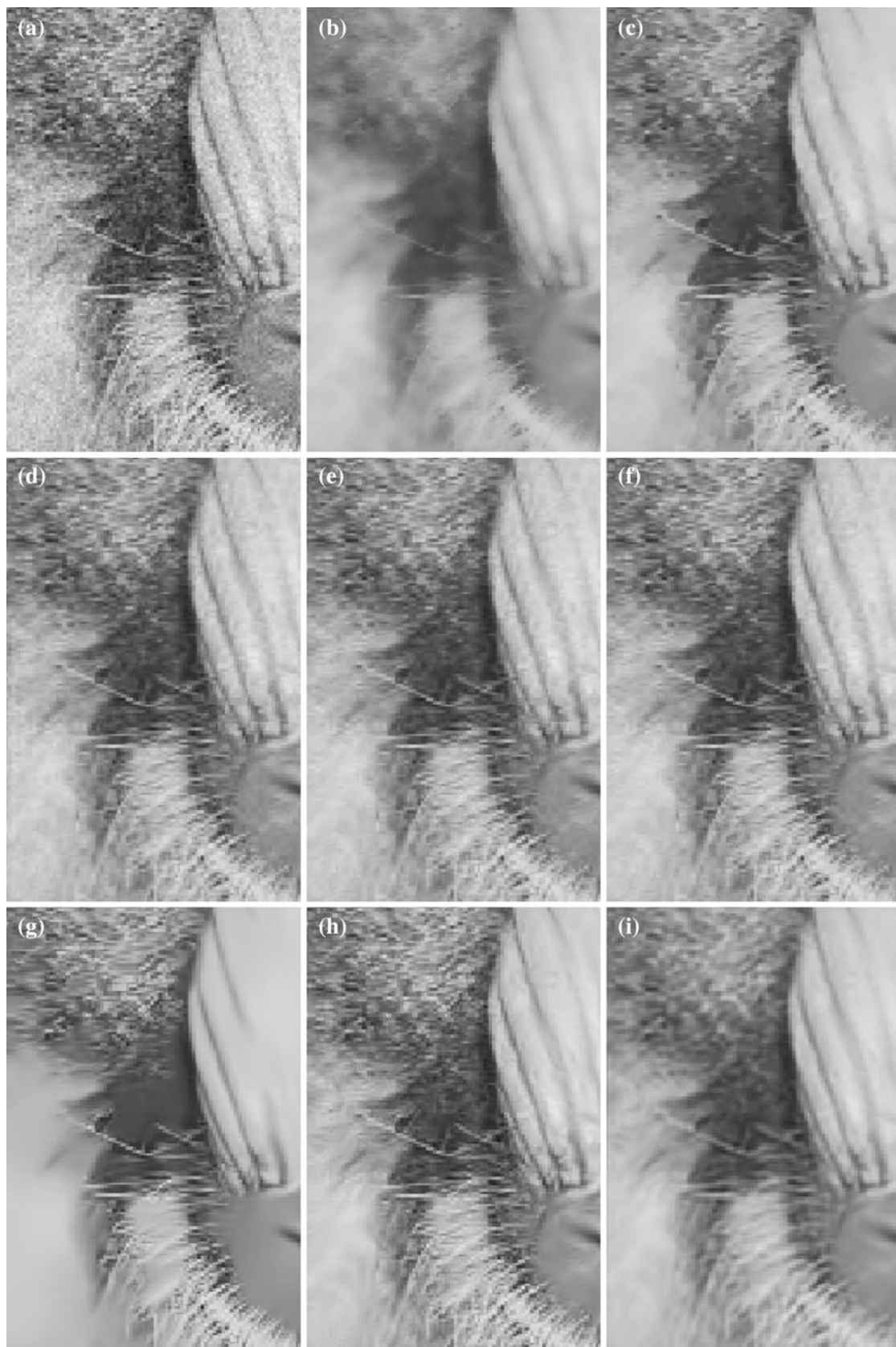
Fig. 5 Noisy baboon image with $\sigma = 50$ and its denoised images by different methods. **a** Noisy image with $\sigma = 50$, denoised images using **b** BF, **c** MRBF, **d** WT, **e** GFMT, **f** BFMT, **g** NL-means, **h** BLSGSM, **i** Kernel based

means, BLS-GSM and Kernel based method are shown in (b), (c), (d), (e), (f), (g), (h) and (i) respectively. Figs. 4 and 5 show the denoised images by different methods for a noisy baboon image with $\sigma = 20$ and 50 respectively. Similarly, Fig. 6 shows *a portion of the denoised image* by different methods for a noisy baboon image with $\sigma = 10$. It is known that the BF removes noise by domain filtering and retains the edges by range filtering but this is at the *cost of image details*. This is observed in Figs. 4b, 5b and 6b that the *image details also have been smoothed along with noise by domain filtering (nose region of the baboon)*. After one level of wavelet decomposition in MRBF, *some image details in the approximation subband have been lost* because of domain filter inherent in BF. Further, like iterated BF, the MRBF also has the *effect of flattening the gray levels in an*

image considerably resulting in a *cartoon-like appearance* [20] due to application of BF after each level of wavelet reconstruction. The *flattening effect of gray levels* and *loss of image details (nose region of the baboon)* can be observed in Figs. 4c, 5c and 6c. But this is not the case with the proposed methods GFMT and BFMT, as the *details lost* because of BF has been *thresholded and added back to get the denoised image* (Figs. 4e, f, 5e, f, 6e, f). Similar to BF, NL-means has removed the image details along with the noise, and the extent of smoothing is too much even with $\sigma = 20$, and for $\sigma = 50$, it has fully blurred the image such that it is difficult to make out the Nostrils and Eyes. The mustache is clearly visible in denoised images by WT (Figs. 4d, 6d), GFMT (Figs. 4e, 6e), BFMT (Figs. 4f, 6f) and BLS-GSM (Figs. 4h, 6h) and looks blurred to some extent in Kernel

Fig. 6 Region of a noisy baboon image with $\sigma = 10$ and its denoised images by different methods. **a** Noisy image with $\sigma = 10$, denoised images using **b** BF, **c** MRBF, **d** WT, **e** GFMT, **f** BFMT, **g** NL-means, **h** BLSGSM, **i** Kernel based
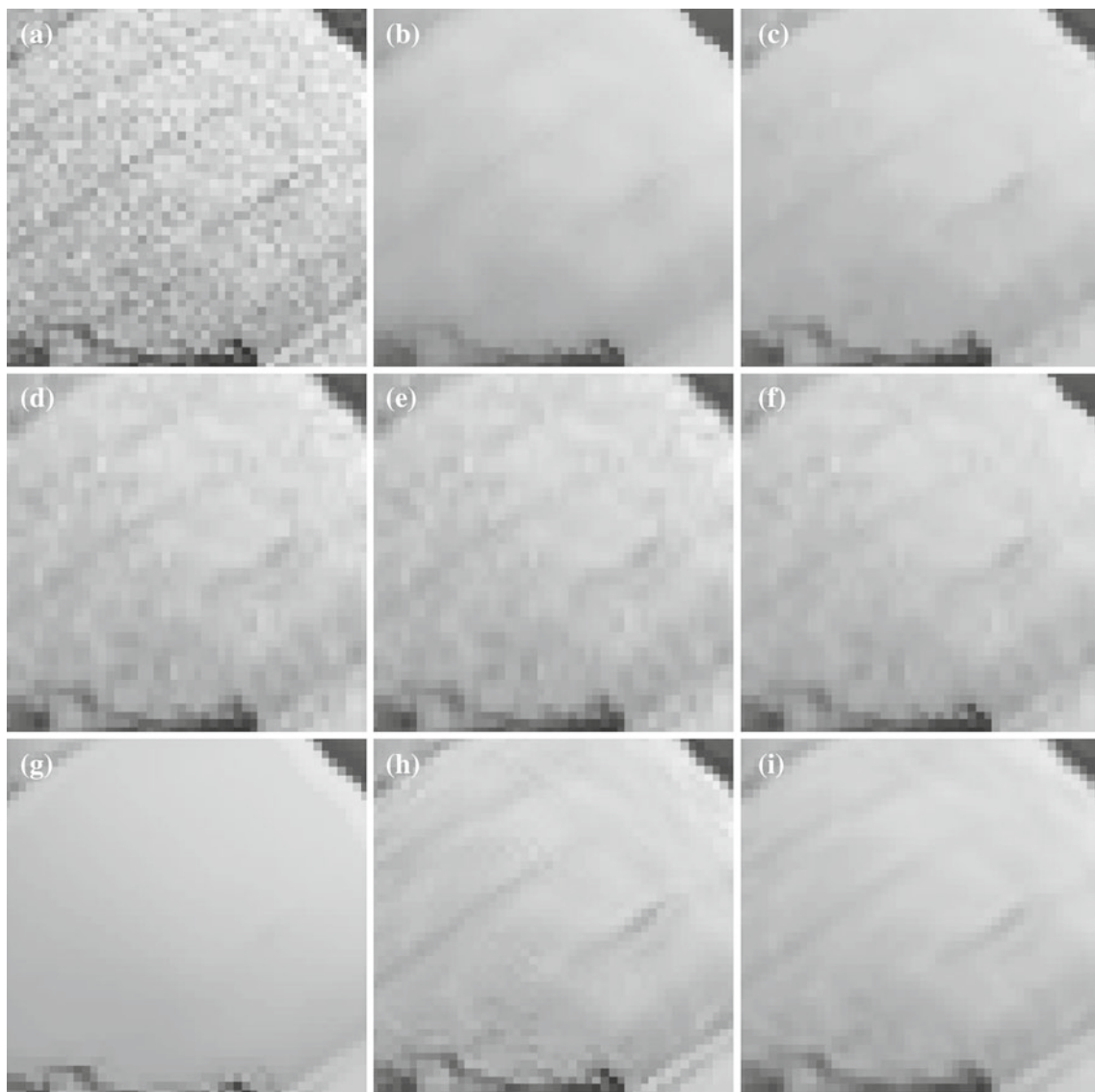
Fig. 7 Region of a noisy Lena image with $\sigma = 10$ and its denoised images by different methods. **a** Noisy image with $\sigma = 10$, denoised images using **b** BF, **c** MRBF, **d** WT, **e** GFMT, **f** BFMT, **g** NL-means, **h** BLSGSM, **i** Kernel based

based (Figs. 4i, 6i), NL-means (Fig. 6g) with $\sigma = 10$) and MRBF (Fig. 6c) with $\sigma = 10$). Further it is observed from Figs. 4 and 6 that, the beard (left bottom portion) is also blurred in all the images except WT, GFMT and BFMT. It is also observed from Figs. 4, 6 that the performance of the GFMT and BFMT is akin to WT in terms of image details and denoising. Also from Fig. 5 it is noticed that, eventhough the image quality of denoised image by BLS-GSM and Kernel based method is good, there is too much blurring near nose portion of the image. In this case, performance of the proposed method is inferior to both BLS-GSM (Fig. 5h) and Kernel based methods (Fig. 5i), and superior to other methods under consideration.

To explain the performance of the proposed methods on different images, *a hat portion the Lena image* is considered

in Fig. 7 with $\sigma = 10$. Here also, the denoised image by both BF and NL-means suffers from the smoothing of noise as well as image details and is shown in Fig. 7b and g respectively. Further, the denoised image by MRBF has *a flattening effect of gray levels* resulting in a *cartoon-like appearance* thereby *loosing image details* (Fig. 7c). It is observed that, the proposed methods have better performance in terms of details and denoising (Fig. 7e, f) as compared to that of BF (Fig. 7b), MRBF (Fig. 7c) and NL-means (Fig. 7g). Among the proposed methods, BFMT (Fig. 7f) has shown better performance in terms of denoising compared to that of GFMT (Fig. 7e) and WT (Fig. 7d). Here also, in terms of image quality, performance of the proposed method is inferior to both BLS-GSM (Fig. 7h) and Kernel based methods (Fig. 7i), and superior to other methods.

Table 2 Performance comparison of different denoising methods in terms of PSNR

σ	10	20	30	40	50	10	20	30	40	50
Input image	Lena 256 × 256					Barbara 256 × 256				
WT	30.77	27.31	25.57	24.50	23.70	29.16	24.79	22.70	21.67	21.15
MRBF	31.34	28.24	**26.66**	**25.60**	**24.67**	28.99	24.55	22.91	**22.23**	21.71
BF	29.28	26.74	25.64	24.85	24.13	24.88	23.17	22.57	22.12	21.69
BLSGSM	**33.23**	29.80	27.87	26.42	25.18	31.66	27.74	25.63	24.11	22.45
Kernel based	30.13	27.98	26.44	25.22	24.18	24.47	23.60	22.85	22.16	21.51
NL-means	33.60	**28.41**	25.84	24.16	22.95	**30.77**	**25.81**	**23.20**	21.53	20.44
GFMT	30.85	27.38	25.68	24.60	23.94	29.00	24.67	22.53	21.72	21.39
BFMT	31.63	27.95	26.11	24.97	24.18	29.16	24.87	22.91	22.16	**21.72**
Input image	Boat 256 × 256					Baboon 256 × 256				
WT	30.94	27.14	25.23	24.04	23.19	28.45	24.58	23.03	22.18	21.61
MRBF	31.58	**27.84**	**25.89**	**24.70**	**23.82**	27.64	24.24	23.02	22.44	22.02
BF	28.20	25.67	24.70	24.02	23.41	24.25	23.21	22.77	22.42	22.07
BLSGSM	32.69	28.99	27.04	25.60	24.42	30.39	26.20	24.29	23.23	22.50
Kernel based	29.69	27.33	25.75	24.57	23.59	25.85	24.34	**23.34**	**22.65**	**22.12**
NL-means	**32.16**	27.13	24.41	23.02	22.16	**29.32**	23.23	21.56	21.00	20.74
GFMT	31.00	27.23	25.24	24.04	23.27	28.37	24.49	22.92	22.21	21.77
BFMT	31.48	27.55	25.51	24.32	23.49	28.58	**24.83**	23.25	22.49	22.01

Table 3 Performance comparison of different denoising methods in terms of IQI

σ	10	20	30	40	50	10	20	30	40	50
Input image	Lena 256 × 256					Barbara 256 × 256				
WT	0.9888	0.9799	0.9711	0.9634	0.9567	0.9846	0.9637	0.9449	0.9331	0.9272
MRBF	**0.9905**	0.9827	0.9768	0.9721	0.9664	0.9834	0.9620	0.9467	**0.9398**	**0.9356**
BF	0.9863	0.9774	0.9718	0.9668	0.9607	0.9637	0.9494	0.9425	0.9387	0.9349
BLSGSM	0.9939	0.9872	0.9813	0.9760	0.9710	0.9914	0.9802	0.9680	0.9572	0.9422
Kernel based	0.9887	**0.9834**	**0.9788**	**0.9729**	**0.9675**	0.9610	0.9535	0.9454	0.9391	0.9332
NL-means	0.9939	0.9831	0.9740	0.9663	0.9585	**0.9890**	**0.9693**	**0.9480**	0.9269	0.9110
GFMT	0.9891	0.9797	0.9713	0.9639	0.9586	0.9839	0.9632	0.9429	0.9341	0.9310
BFMT	**0.9905**	0.9808	0.9729	0.9650	0.9589	0.9841	0.9644	0.9473	0.9389	0.9349
Input image	Boat 256 × 256					Baboon 256 × 256				
WT	0.9889	0.9746	0.9624	0.9486	0.9398	0.9730	0.9403	0.9171	0.9011	0.8885
MRBF	0.9898	**0.9803**	**0.9727**	0.9644	0.9562	0.9687	0.9363	0.9183	0.9076	0.8989
BF	0.9832	0.9733	0.9662	0.9560	0.9462	0.9381	0.9229	0.9145	0.9071	0.8995
BLSGSM	0.9931	0.9840	0.9768	0.9694	0.9634	0.9820	0.9561	0.9357	0.9211	0.9097
Kernel based	0.9875	0.9792	0.9726	**0.9664**	**0.9615**	0.9548	0.9357	0.9215	**0.9110**	**0.9014**
NL-means	0.9881	0.9726	0.9619	0.9521	0.9444	**0.9743**	0.9227	0.8873	0.8746	0.8707
GFMT	0.9892	0.9762	0.9653	0.9514	0.9411	0.9726	0.9389	0.9163	0.9024	0.8913
BFMT	**0.9903**	0.9780	0.9668	0.9533	0.9424	0.9735	**0.9429**	**0.9219**	0.9074	0.8970

The performances of the proposed methods are measured quantitatively using PSNR, Image Quality Index (IQI) [35] and Visual Fidelity Index (VIF) [36] of the denoised images. PSNR, IQI and VIF of the denoised images by different methods are tabulated in Tables 2, 3 and 4 respectively. As BLS-GSM has a good denoising performance, it has highest values in terms of PSNR, IQI and VIF. By excluding BLS-GSM, the

proposed methods are compared and discussed with other methods under consideration and hence the second highest PSNR, IQI and VIF values are bolded.

It is observed from the Table 2 that, the denoised images by MRBF has highest PSNR than that of the other methods for images like Lena ($\sigma = 30, 40, 50$), Boat ($\sigma = 20, 30, 40, 50$) and Barbara ($\sigma = 40$). Similarly, NL-

Table 4 Performance comparison of different denoising methods in terms of VIF

σ	10	20	30	40	50	10	20	30	40	50
Input image	Lena 256 × 256					Barbara 256 × 256				
WT	0.4971	0.3097	0.2254	0.1781	0.1485	0.4944	0.3109	0.2278	0.1797	0.1505
MRBF	0.5047	0.3463	0.2705	0.2245	0.1907	0.5130	0.3541	0.2777	**0.2293**	**0.1942**
BF	0.4298	0.3010	0.2407	0.2030	0.1758	0.4023	0.2947	0.2434	0.2079	0.1808
BLSGSM	**0.5600**	0.3871	0.2999	0.2453	0.2015	0.5726	0.3971	0.3114	0.2561	0.2081
Kernel based	0.5101	**0.3534**	**0.2744**	**0.2257**	**0.1914**	0.5085	**0.3555**	**0.2787**	0.2288	0.1929
NL-means	0.5646	0.3248	0.2341	0.1722	0.1280	**0.5186**	0.3121	0.2183	0.1598	0.1166
GFMT	0.4921	0.3049	0.2269	0.1874	0.1640	0.4840	0.3018	0.2239	0.1900	0.1693
BFMT	0.5039	0.3213	0.2423	0.2010	0.1735	0.4930	0.3142	0.2410	0.2041	0.1784
Input image	Boat 256 × 256					Baboon 256 × 256				
WT	0.5155	0.3182	0.2279	0.1757	0.1396	0.4715	0.2664	0.1755	0.1264	0.0943
MRBF	0.5263	**0.3414**	**0.2548**	**0.2047**	**0.1713**	0.4435	0.2662	0.1907	0.1500	0.1231
BF	0.4014	0.2750	0.2191	0.1850	0.1606	0.3142	0.2234	0.1766	0.1457	0.1229
BLSGSM	0.5575	0.3697	0.2793	0.2228	0.1791	0.5206	0.3176	0.2224	0.1688	0.1332
Kernel based	0.4968	0.3332	0.2522	0.2021	0.1662	0.4650	**0.2917**	**0.2096**	**0.1612**	**0.1285**
NL-means	**0.5369**	0.2791	0.1633	0.1094	0.0799	**0.4923**	0.1767	0.0786	0.0474	0.0345
GFMT	0.5142	0.3158	0.2242	0.1755	0.1477	0.4635	0.2591	0.1728	0.1326	0.1094
BFMT	0.5223	0.3246	0.2346	0.1880	0.1598	0.4692	0.2693	0.1869	0.1456	0.1209

means has highest PSNR for images like Lena ($\sigma = 20$), Barbara ($\sigma = 10, 20, 30$), Boat ($\sigma = 10$) and baboon ($\sigma = 10$), whereas Kernel based method has highest PSNR only for baboon image with ($\sigma = 30, 40, 50$). In many cases, BFMT is a closest competitor for MRBF or NL-means filter and stood second in the list when BLS-GSM is excluded for comparison. Further, BFMT stood first in the list with highest PSNR for Baboon ($\sigma = 20$) and Barbara ($\sigma = 50$) images.

From Table 3 it noticed that, almost all the IQI values for different methods are greater than 0.9 and approaching 1. This means, when the IQI approaches 1 the denoised image is close to original image. Here, the denoised images by Kernel based has highest IQI than that of the other methods for images like Lena ($\sigma = 20, 30, 40, 50$), Boat ($\sigma = 40, 50$) and Baboon ($\sigma = 40, 50$). Likewise, MRBF has highest IQI for Lena ($\sigma = 10$), Barbara ($\sigma = 40, 50$) and Boat ($\sigma = 20, 30$) images, whereas NL-means has highest IQI for Barbara ($\sigma = 10, 20, 30$) and Baboon ($\sigma = 10$) images. The proposed method BFMT has highest IQI for Lena ($\sigma = 10$), Boat ($\sigma = 10$) and Baboon ($\sigma = 20, 30$) images. Further, in most cases of IQI, BFMT stood second in the list (excluding BLG-GSM).

It is noticed from Table 4 that, Kernel based has highest VIF for Lena ($\sigma = 20, 30, 40, 50$), Barbara ($\sigma = 20, 30$) and Baboon ($\sigma = 20, 30, 40, 50$) images. Similarly, MRBF has highest VIF for Barbara ($\sigma = 40, 50$) and Boat ($\sigma = 20, 30, 40, 50$) images, whereas NL-means has highest IQI for Barbara ($\sigma = 10$), Boat ($\sigma = 10$) and Baboon ($\sigma = 10$). Here also, the denoised image is close to original image if

Table 5 Timing complexity of different denoising methods

Method	Time (S) 256 × 256
WT	0.31
MRBF	1.60
BF	0.98
BLG-GSM	7.27
Kernels based	36.45
NL-means	51.13
G/BFMT	1.30

VIF approaches 1. From Tables 2, 3 and 4 it is observed that, within the two proposed methods, BFMT scores over GFMT in terms of PSNR, IQI and VIF.

To briefly compare the complexity of proposed methods and considered methods, the time consumed by each method is tabulated in Table 5. It is observed that, image denoising by WT requires less time followed by BF, G/BFMT, MRBF, BLG-GSM, Kernel based and NL-means in last. With this it can be inferred that, the complexity of the proposed method is inferior to WT and BF, and superior to MRBF, BLG-GSM, Kernel based and NL-means. Hence there is a trade-off between the performance and complexity of the denoising methods.

5 Conclusions and future work

In this paper, the amalgamation of Gaussian/bilateral filter and its method noise thresholding using wavelets has

been proposed. The performance of the proposed methods is compared with WT, BF, MRBF, NL-means, BLS-GSM and Kernel based methods. Through experiments conducted on standard images it was found that, BLS-GSM has shown a good denoising performance in terms of visual quality, PSNR, IQI and VIF but at the cost of increased computational complexity. With lesser computational complexity, the proposed methods have shown a similar performance as that of WT and superior/comparable performance to that of BF, MRBF, NL-means and Kernel based methods, in terms of method noise, visual quality, PSNR and IQI.

The performance of the proposed method can be improved by using shift invariant wavelet transform or steerable wavelet transform for method noise decomposition with better threshold value computation and thresholding techniques. These issues and modification of the proposed framework for non-Gaussian noise scenarios as well as the application of other non-linear filters instead of BF are left as future work and will inspire further research towards understanding and eliminating noise in real images.

References

1. Gonzalez, R.C., Woods, R.E.: Digital Image Process. Pearson Education (Singapore) Pte. Ltd., Delhi, India (2004)
2. Ghazel, M.: Adaptive Fractal and Wavelet Image Denoising. PhD thesis, Department of Electrical & Computer Engineering, University of Waterloo, Ontario, Canada (2004)
3. Chang, S.G., Yu, B., Vetterli, M.: Adaptive wavelet thresholding for image denoising and compression. IEEE Trans. Image Process. **9**(9), 1532–1546 (2000)
4. Jansen, M.: Wavelet Thresholding and Noise Reduction. PhD thesis, Department of Computer Science, Katholieke Universiteit Leuven, Heverlee, Belgium (2000)
5. Şendur, L., Selesnick, I.W.: Bivariate shrinkage functions for wavelet-based denoising exploiting interscale dependency. IEEE Trans. Signal Process. **50**(11), 2744–2756 (2002)
6. Fang, H.-T., Huang, D.-S.: Wavelet de-noising by means of trimmed thresholding. In: Proceedings of the 5th World Congress on Intelligent Control and Automation, vol. 2, pp. 1621–1624. Hangzhou, P. R. China (2004)
7. Zong, X., Laine, A.F., Geiser, E.A., Wilson, D.C.: De-noising and contrast enhancement via wavelet shrinkage and nonlinear adaptive gain. Wavelet applications III. In: Proceedings of SPIE, vol. 2762, pp. 566–574. Orlando, FL (1996)
8. Marpe, D., Cycon, H.L., Zander, G., Barthel, K.-U.: Context-based denoising of images using iterative wavelet thresholding. In: Proceedings of SPIE on Visual Communications and Image Process, vol. 4671, pp. 907–914 (2002)
9. Cristobal, G., Cuesta, J., Cohen, L.: Image filtering and denoising through the scale transform. In: IEEE Proceedings of International Symposium on Time-Frequency and Time-Scale Analysis, pp. 617–620, Pittsburgh, PA (1998)
10. Donoho, D.L., Johnstone, I.M.: Ideal spatial adaptation via wavelet shrinkage. Biometrika **81**(3), 425–455 (1994)
11. Donoho, D.L.: Denoising by soft thresholding. IEEE Trans. Inform. Theory **41**(3), 613–627 (1995)
12. Chang, S.G., Yu, B., Vetterli, M.: Spatially adaptive thresholding with context modeling for image denoising. IEEE Trans. Image Process. **9**(9), 1522–1531 (2000)
13. Pizurica, A., Philips, W.: Estimating the probability of the presence of a signal of interest in multiresolution single and multiband image denoising. IEEE Trans. Image Process. **15**(3), 654–665 (2006)
14. Bruni, V., Piccoli, B., Vitulano, D.: A fast computation method for time scale signal denoising. Signal Image Video Process. **3**(1), 63–83 (2009). doi:10.1007/s11760-008-0060-9
15. Daubechies, I.: Ten lectures on wavelets. In: CBMS-NSF Regional Conference Series in Applied Mathematics, vol. 61, 2nd edn. SIAM, Philadelphia, USA (1992)
16. Mallat, S.: A Wavelet Tour of Signal Processing. Academic Press, New York (1998)
17. Donoho, D.L., Johstone, I.M.: Adapting to unknown smoothness via wavelet shrinkage. J. Am. Stat. Assoc. **90**(432), 1200–1224 (1995)
18. Portilla, J., Strela, V., Wainwright, M.J., Simoncelli, Eero P.: Image denoising using scale mixtures of Gaussians in the wavelet domain. IEEE Trans. Image Process. **12**(11), 1338–1351 (2003)
19. Laparra, V., Gutierrez, J., Camps-Valls, G., Malo, J.: Image denoising with kernels based on natural image relations. J. Mach. Learn. Res. **11**, 873–903 (2010)
20. Tomasi, C., Manduchi, R.: Bilateral filtering for gray and color images. In: Proceedings of International Conference Computer Vision, pp. 839–846 (1998)
21. Smith, S.M., Brady, J.M.: Susan—a new approach to low level image processing. Int. J. Comput. Vis. **23**(1), 45–78 (1997)
22. Yaroslavsky, L.: Digital Picture Processing—An Introduction. Springer, New York (1985)
23. Morillas, S., Gregori, V. and Sapena, A.: Fuzzy bilateral filtering for color images. Lecture Notes in Computer Science, pp. 138–145(2006)
24. Overton, K.J., Weymouth, T. E.: A noise reducing preprocessing algorithm. IEEE Proceedings of Computer Science Conference Pattern Recognition and Image Process, pp. 498–507 (1979)
25. Perona, P., Malik, J.: Scale-space and edge detection using anisotropic diffusion. IEEE Trans. PAMI. **12**(7), 629–639 (1990)
26. Zhang, B., Allebach, J.P.: Adaptive bilateral filter for sharpness enhancement and noise removal. IEEE Trans. Image Process. **17**(5), 664–678 (2008)
27. Eisemann, E., Durand, F.: Flash photography enhancement via intrinsic relighting. Proceedings of the SIGGRAPH Conference, ACM Transactions on Graphics, vol. 23, no. 3 (2004)
28. Barash, D.: A fundamental relationship between bilateral filtering, adaptive smoothing, and the nonlinear diffusion equation. IEEE Trans. PAMI **24**(6), 844–847 (2002)
29. Elad, M.: On the origin of the bilateral filter and ways to improve it. IEEE Trans. Image Process. **11**(10), 1141–1151 (2002)
30. Buades, A., Coll, B., Morel, J.M.: A review of image denoising methods, with a new one. Multiscale Model. Simul. **4**(2), 490–530 (2005)
31. Kervrann, C., Boulanger, J.: Optimal spatial adaptation for patch-based image denoising. IEEE Trans. Image Process. **15**(10), 2866–2878 (2006)
32. Zhang, M., Gunturk, B.K.: Multiresolution bilateral filtering for image denoising. IEEE Trans. Image Process. **17**(12), 2324–2333 (2008)

33. Wenxuan, S., Jie, L., Minyuan, W.: An image denoising method based on multiscale wavelet thresholding and bilateral filtering. Wuhan Univ. J. Nat. Sci. **15**(2), 148–152 (2010)

34. Mustafa, Z.A., Kadah, Y.M.: Multi Resolution Bilateral Filter for MR Image Denoising. In: Proceedings of 1st Middle East Conference on Biomedical Engineering (MECBME), pp. 180–184, Sharjah, UAE, (2011)

35. Roy, S., Sinha, N., Sen, A.K.: A new hybrid image denoising method. Int. J. Inform. Technol. Knowl. Manag. **2**(2), 491–497 (2010)

36. Sheikh, H.R., Bovik, A.C.: Image information and visual quality. IEEE Trans. Image Process. **15**(2), 430–444 (2006)